ISSN 1392-1320 MATERIALS SCIENCE (MEDŽIAGOTYRA). Vol. XX, No. X. 2025

Theoretical Design of Asymmetric/symmetric Nanodisk Arrays Deposited on GaAs Film for Plasmonic Modulation and Sensing

Cheng SUN [1, 2], Xue YANG [1, 2], Xinyu LI [1, 2], Shuwen CHU [1, 2] *

[1] *College of Physical Science and Technology, Dalian University, 116622, China*
[2] *Liaoning Engineering Laboratory of Optoelectronic Information Technology, Dalian, 116622, China*

http://doi.org/10.5755/j02.ms.38239

Received 29 July 2024; accepted 4 November 2024

Metallic plasmonic nanostructures can achieve nanoscale light-matter interactions and have a wide range of applications in spectral modulation and optical sensing fields stemming from their rich and tunable optical properties. Herein, we propose a composite nanostructure consisting of a gold nanodisk array and a GaAs thin film, which achieves symmetric and asymmetric configurations by adjusting the nanodisk radius of the array structure. We systematically investigate the relationship between plasmonic modulation and asymmetric/symmetric coupling modes. The results indicate that the two configurations correspond to single resonance and dual resonance, respectively. The short wavelength of the dual-resonant mode is jointly excited by the local surface plasmon polariton (LSP) mode of the nanodisk itself and the waveguide-hybridized lattice mode of the bottom GaAs film. And the long wavelength corresponds to the LSP mode of the array nanostructure which strongly depends on its size. Improving structural symmetry leads to different trends in resonance wavelength. Furthermore, we investigate the sensing performances for asymmetric/symmetric nanodisk arrays. This work is of great significance for applications such as multi-resonance sensing, plasmonic modulation, etc.
Keywords: asymmetric/symmetric nanodisk array, single-/dual-resonant mode, finite difference time domain, sensing performance.

1. INTRODUCTION

Surface Plasmons (SPs) are electromagnetic oscillations that excite and couples charge density fluctuations at the metal dielectric interface [1]. So far, there are many applications based on SPs, including controlling electromagnetic fields, absorption-induced transparency (AIT), imaging, and sensing, etc. For example, the freedom of design based on metamaterials was used to control the electromagnetic field flexibly, that is, to achieve the directional transmission direction and local configuration artificially [2]. The plasmonic nanostructure with precisely filling subwavelength diameter nanoholes in a silver film with dielectric material demonstrated an AIT effect in both experiments and numerical simulations [3]. Metasurface-based imaging modalities and features of metalenses for imaging could closely approximate the ideal phase of a perfect lens to focus light at the theoretical fundamental diffraction limit without spherical aberrations [4]. A novel platform based on all dielectric metasurfaces was proposed and demonstrated for large-scale parallel sensing of trace biomolecules in hyperspectral imaging, which originated from geometrically adjustable high-quality factor bound states in continuous medium (BIC) excitation resonance in near-infrared region [5].

Recently, many groups have confirmed the size and shape of the nanostructures, the nature of the substrate, or the surrounding medium to access excitation of different wavelength bands and resonance modes. To date, in addition to symmetric systems, introducing asymmetry to generate mode coupling and hybridization has gradually become a research hotspot. For instance, a thorough review of the recent research progress on achieving high-quality (high-Q) factor plasmonic resonances was provided, by emphasizing the fundamentals and six resonant mode types; the applications of high-Q plasmonic resonances were also discussed in Ref. [6]. Based on lineshape engineering, the Fano resonances with sharp asymmetric profiles exhibited a small linewidth and a high spectral contrast by exploiting different mechanisms and designing various metallic nanostructures [7]. In addition, the near-field of the structure could also be greatly enhanced at the desired frequency [8]. By introducing a conducting metal layer underneath a Fano resonant asymmetric ring/disk plasmonic nanocavity system, it was demonstrated that the electromagnetic field could be strongly enhanced [9]. A novel approach to exceptional points (EPs) based on spatial symmetry breaking was proposed. The plasmonic EPs were based on the hybridization of detuned resonances in multilayered plasmonic structures to reach a critical complex coupling rate between nanoantenna arrays, resulting in the simultaneous coalescence of the resonances and loss rates [10]. The possibility to maximize or cancel the interaction between the hybridized surface lattice resonances (SLRs) by simply controlling the distance between particles was demonstrated through surfaces made of binary arrays with unit cells made of two gold disks of distinct diameters [11]. The narrow-band decapole resonance modes in gold nanohole arrays fabricated by scalable colloidal lithography were studied. The high quality of this resonance associated with highly accessible large local electromagnetic fields offered high refractive

* Corresponding author. Tel.: +86-411-87402712; fax: +86-411-87402712. E-mail: *chushuwen@dlu.edu.cn* (S. Chu)

index sensitivity [12]. A strategy was based on the hybridization of Mie SLRs in periodic silicon bipartite nanodisk arrays, of which the central nanodisk was displaced from the center of the unit cell. It demonstrated a novel strategy to achieve dual-band symmetry-protected BIC in silicon metasurfaces [13]. The bipartite nanoparticle arrays depending on the relative position of the two particles within the unit cell can support SLRs with a super- or subradiant character. The results of this work provide an efficient approach to obtain narrow linewidths that are robust to fabrication imperfections [14].

Among dielectric materials, GaAs is a promising one that may also have great application potentials in plasmonics. For example, it is obvious local surface plasmon polariton (LSP) mode can be realized in the proposed triangular prism meta-antennas, and the resonant wavelength, electromagnetic field distribution, surface charge distribution, and surface current density can be effectively tuned by structural and material parameters [15]. GaAs can also be used to make GaAs solar cells. Due to its direct and widely accessible bandgap energy, excellent photophysical properties to generate, transport, and collect charge carriers by interacting with sunlight, and ability to form monolithically grown multijunction tandem systems [16].

In this work, we demonstrate symmetric/asymmetric gold (Au) disk nano arrays covered on GaAs substrate. The influence of nanodisk radius and substrate thickness on the reflection spectra of the structure are studied. By changing the asymmetry of the plasmonic nanostructure, the position and mode of resonant wavelengths can be altered. With the help of the distribution of electromagnetic fields at resonance wavelengths, the article analyzes the physical mechanism. In addition, the sensing performance of the structure has been studied by changing the refractive index of the environment.

2. STRUCTURE AND METHOD

Fig. 1 schematically shows the asymmetric nanodisk array deposited on the GaAs layer. The substrate is silicon dioxide (SiO_2). The asymmetry of this structure is achieved by the radius of a small nanodisk (R). The large nanodisk radius has been fixed at r = 140 nm. Since R = 140 nm, the corresponding structure is symmetric. This structure is distributed in a triangular array and its constant is set at P = 450 nm along the X axis. The height of the disks is h with the dielectric coefficient by Lorentz-Drude Mode [17]. The thickness of the GaAs layer is H with a refractive index by Palik [18]. All the spectra were recorded in water (n = 1.3313) as the superstrate. Wherein, the GaAs layer serves as a dielectric layer and interacts with the gold nanodisk, coupling and exciting new resonance modes. We adopt the finite difference time domain (FDTD) method to perform reflection spectra and the near-field distributions [19]. An x-polarized plane-wave light is incident along the negative z-axis, in the wavelength range of 400 - 1000nm. To avoid the possible artifacts that might be induced by the simulation method, the mesh size was always kept smaller than 1/10 of the shortest wavelength studied in the simulation region of non-plasmon-carrying media. Periodic boundary conditions are applied in the x and y directions, and perfect matching layer (PML) boundary conditions are used in the z directions. Note that no error estimates are given in this work, since the results are all calculated by using simulations, and they need to be used with caution, especially when compared with experimental data.

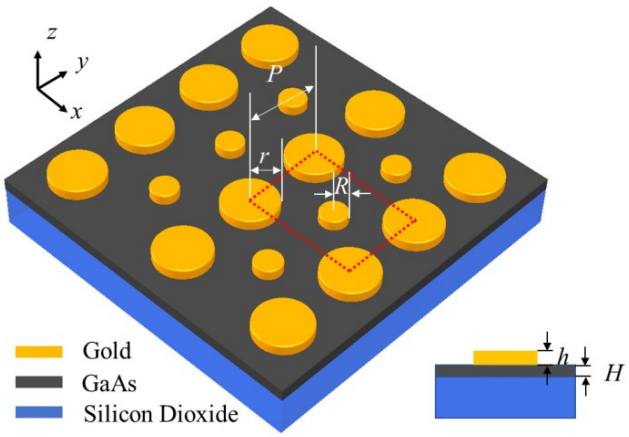

Fig. 1. Schematic diagram of the asymmetric nanodisk array fabricated on GaAs/SiO_2 layers. The small radius of nanodisks is R, the large radius of disks is r, the height of the disks is h and the thickness of the GaAs layer is H. The lattice constant is P. The illustration in the bottom right corner is a two-dimensional view

3. RESULTS AND DISCUSSION

3.1. Varied radius of the large disks

To evaluate the optical properties, we investigate the influence of different parameters on the reflectance spectra. As shown in Fig. 2, while other parameters remain fixed, the position and intensity of the resonance wavelength change since the large radius of the nanodisk (R) increases. Fig. 2 a displays the calculated spectra of the asymmetric nanodisk array with R varies from 20 nm to 100 nm. There are two obvious resonance dips in the range of 600 nm to 800 nm, namely λ_1, and λ_2. As the radius R increases, the resonance depth of the resonance dip at position λ_1 gradually increases. On the contrary, the resonance depth of the resonance dip at position λ_2 gradually decreases. When R = 100 nm, the dip at λ_2 is almost invisible. It is worth noting that the wavelength position has hardly changed within this range.

Fig. 2 b shows the change of reflectance spectra when the radius R increases from 100 nm to 200 nm. It can be seen that there is only one resonance dipλ_1. And the intensity of the resonance dip attains maximum and strong resonant coupling with the incident light when R = 140 nm, corresponding to the case that the radius of the large disk is equal to that of the small disks. When R = 200 nm, the trend of exciting new resonance modes near λ_2 occurs. Comparing the changes in two resonant wavelengths, the dip at λ_1 is forming of LSP mode excited by the structural configuration. And the dip at λ_2 is introduced by the asymmetry systems. That is, as the degree of asymmetry increases, this mode becomes more pronounced. The resonant wavelength at 850 nm originates from the weak coupling of the disks. Due to its lower peak contrast being

difficult to detect in the experiment, the mode is not discussed in the following sensing section.

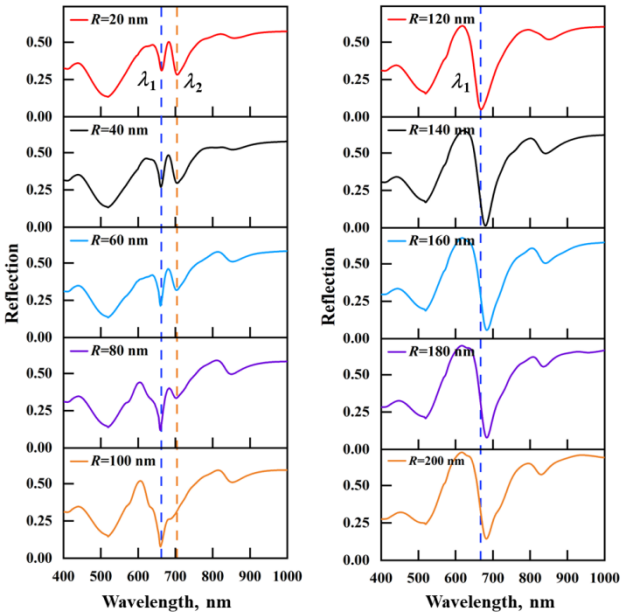

Fig. 2. Reflectance spectra of the proposed plasmonic nanostructure for the distinct radius of the large disks (R): from 20 nm to 200 nm. The height of the disks (h) and the thickness of the GaAs layer (H) remain 50 nm and 60 nm, respectively. The blue dashed line represents the vicinity of wavelength position λ_1, and the orange dashed line represents the vicinity of wavelength position λ_2. a – R varies from 20 nm to 100 nm; b – R varies from 120 nm to 200 nm

3.2. Varied thickness of nanodisk array

Fig. 3 compares R is equal to 20 nm and 140 nm reflectance spectra for different thicknesses of disks h. Results show that in Fig. 3 a, as h increases from 30 nm to 70 nm in the step of 10 nm, the resonance λ_2 is slightly red-shifted, whereas that of the resonance λ_1 experience minimum red-shift. The depth of the resonance wavelengths deepens with the increasing thickness of the Au disks. But at the same time, the width of the resonance dip λ_2 will also increase, while resonance dip λ_1 is exactly the opposite. For the case of R = 140 nm, the redshift is the highest (Fig. 3 b). The resonance depth deepens and the spectral line width widens with the increase of the thickness of the gold disk. This phenomenon is attributed to the introduction of multi-level resonance modes caused by the increase in the thickness of disks. The results indicate that regardless of whether the structure is symmetrical or asymmetrical, changing the thickness of Au disks almost does not affect the overall shape of the spectral lines, but has a significant impact on the resonance position and intensity.

3.3. Varied thickness of GaAs layer

Moreover, the optical properties of the asymmetric nanodisk array under different thickness of the GaAs layer are shown in Fig. 4. Herein, the other structural parameters remain consistent. We investigate the reflection of GaAs layers with thicknesses of H = 20 nm, 40 nm, 60 nm, and 80 nm.

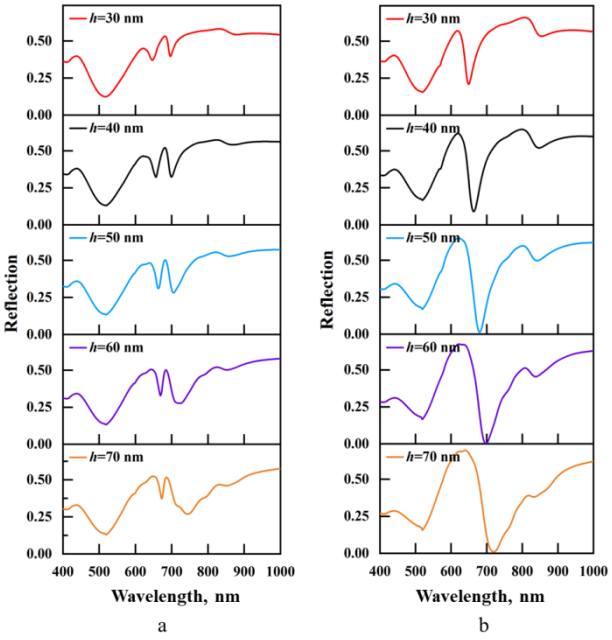

Fig. 3. Simulated reflectance spectra of proposed nanodisk arrays with different thickness of disks. The structural parameters are P = 450 nm, r = 140 nm, H = 60 nm. a – R = 20 nm; b – R = 140 nm

As shown in Fig. 4 a, two main reflection dips are observed for the plasmonic nanostructure with R = 20 nm.

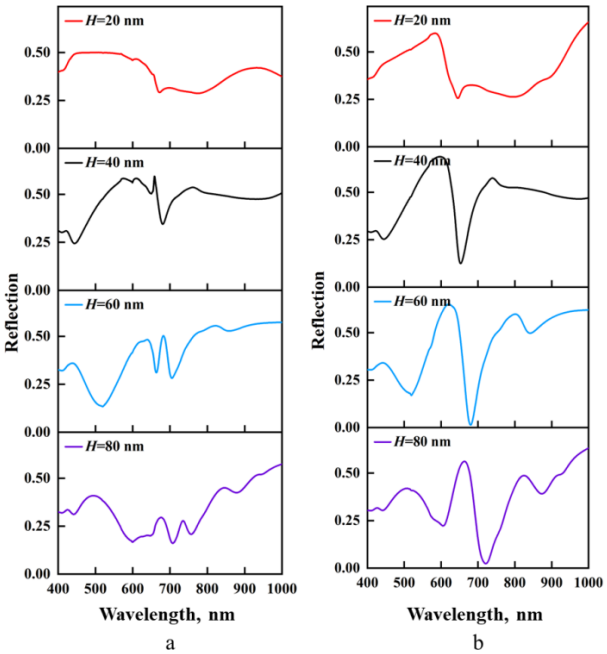

Fig. 4. Optical properties of the asymmetric nanodisk array formed by the Au with GaAs layer (H) changed from 20 nm to 40, 60, and 80 nm, respectively. The structural parameters are P = 450 nm, r = 140 nm, h = 50 nm. a – R = 20 nm; b – R = 140 nm

And as the thickness increases, both resonance wavelengths undergo red shift. Moreover, the 60-nm-thick GaAs layer has the highest resonance intensity and the 60-

nm-thick GaAs layer only appears a weak resonance λ_1. Similarly, the smaller the thickness, the lower the resonance intensity when $R = 160$ nm (Fig. 4 b). However, at this radius size, only one resonant wavelength is present. When $H = 80$ nm, the resonance dip wavelength has already redshifted to nearly 750 nm. It indicates that the optical field coupling and confinement between metal nanostructures and GaAs film depend on the thickness of the film. Especially wavelength λ_1 is more dependent on this parameter variation.

3.4. Distribution of electric field at resonance wavelength

To understand the details of asymmetric/symmetric nanodisk arrays, the electric field distributions for λ_1 and λ_2 are shown in Fig. 5. Normalized field distributions for the nanostructure under the resonant wavelengths in the x–y and x-z plane. As shown in Fig. 5 a, the blue dashed line corresponds to the resonance wavelength λ_1 for $R = 20$ nm.

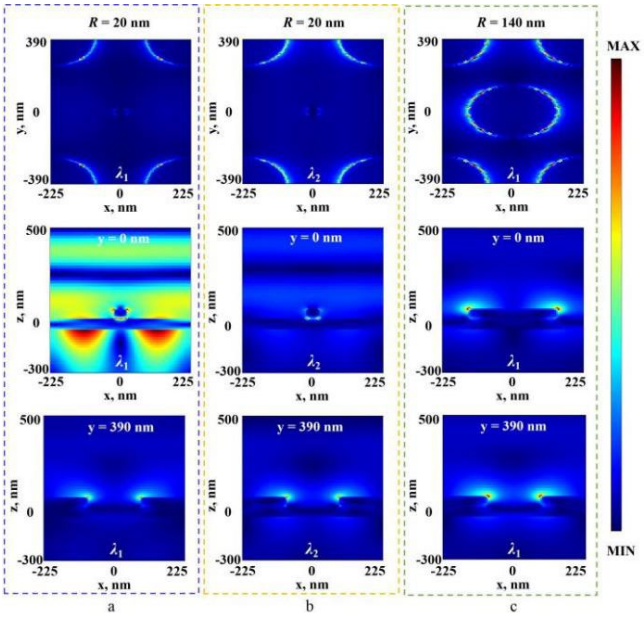

Fig. 5. Normalized field distributions for the two nanostructures under the resonant wavelengths in the x-y, x-z plane of y = 0 nm and y = 390 nm. a – λ_1 for $R = 20$ nm; b – λ_2 for $R = 20$ nm; c – λ_1 for $R = 140$ nm

The electric field is mainly concentrated at the edges of the top surfaces of the small and large nanodisks, as well as the bottom surface of the GaAs film. The former conforms to LSP mode distribution. Meanwhile, this field distribution is excited by the coupling between the large nanodisk and the small nanodisks, resulting in waveguide-hybridized lattice mode on the bottom surface of the GaAs film [20]. Therefore, this resonant dip is coupled with the two modes [21].

The orange dashed line corresponds to the resonance wavelength λ_2 for $R = 20$ nm (Fig. 5 b). The electric field is primarily localized at the two edges of the top surface of the nanodisk, forming LSP mode. The local electromagnetic field supported by metallic features depends critically on the geometric shape and size of the nanostructure at the resonant frequency of the dipole the nanostructure, and this trend becomes more significant as the asymmetry intensifies. As shown in Fig. 5 c, the green dashed line corresponds to the resonance wavelength λ_1 for $R = 140$ nm. In this case, the radius of each nanodisk remains consistent. And the electric field is localized at the edge of each nanodisk, to is typical of LSP mode excitation, according with previous studies. That is to say, the introduction of asymmetric structures reduces the excitation of waveguide-hybridized lattice mode modes.

3.5. Sensing performance

Here, we numerically investigate the sensing performance of our proposed plasmonic nanostructures. In this work, the refractive index of the medium environment is adjusted from 1.3313 to 1.38 to analyze the influence of refractive index on the characteristics of this nanostructure. Extracted resonance wavelengths as a function of refractive index as shown in Fig. 6. We discuss the sensitivity of resonance wavelength under symmetric and asymmetric conditions separately. The bulk sensitivities (S), which can be determined by [16]:

$$S = \Delta\lambda / \Delta n, \quad (1)$$

where $\Delta\lambda$ is the magnitude of resonance wavelength variation; Δn is the change in refractive index.

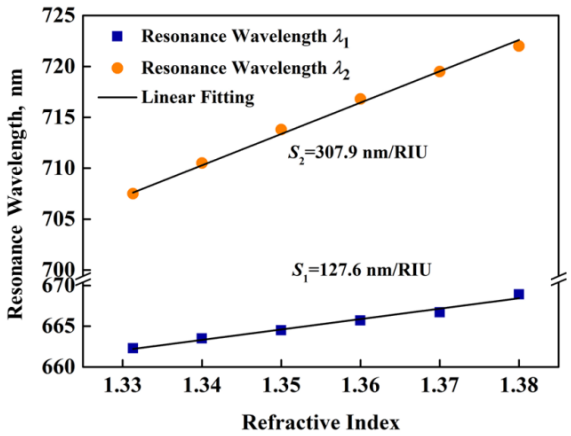

Fig. 6. Refractive index sensing performance of asymmetric nanostructure based on the nanodisk array ($R = 20$ nm). Extracted resonance wavelengths as a function of refractive index

In Fig. 6, when the radius is $R = 20$ nm, two plasmonic resonance wavelengths are observed. And both wavelengths have a redshift with the increase of the refractive index. The sensitivity are $S_1 = 127.6$ nm/RIU and $S_2 = 307.9$ nm/RIU. Regarding Fig. 7, when the radius is $R = 140$ nm, only one resonance wavelength appears in the range of 680 – 700 nm. Similarly, the wavelength redshifts as the refractive index is raised, and its sensitivity factor is determined to be $S_{1*} = 342.1$ nm/RIU. By comparing the value of S_{1*} with those of S_1 and S_2, it is clear that the sensitivity is higher when the center radius of the Au disk is 140 nm. The larger the radius of the large disk, the higher the sensitivity of wavelength λ_1. However, the sum of the double resonance sensitivity of asymmetric structures is greater than the single wavelength resonance sensitivity of symmetric structures [22].

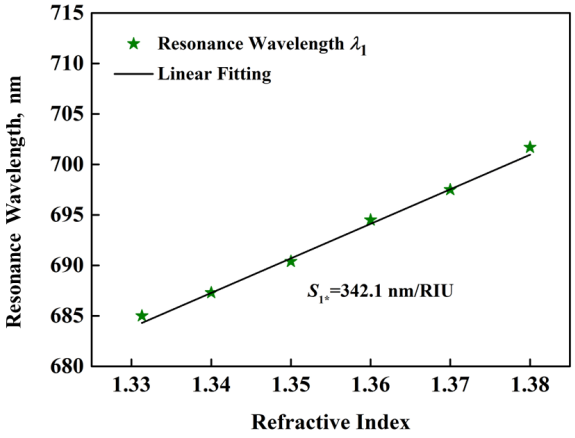

Fig. 7. Refractive index sensing performance of symmetric nanostructure based on the nanodisk array (R = 140 nm). Extracted resonance wavelengths as a function of refractive index

4. CONCLUSIONS

In conclusion, we have proposed and demonstrated a novel strategy to realize a dual-resonant asymmetric nanodisk array and single-resonant symmetric nanodisk array based on GaAs film, which utilizes mode coupling by adjusting the nanodisk radius of the array structure. These resonant modes can be modulated by both the thickness of the GaAs substrate and the Au nanodisk array. We demonstrate that both two systems enable reliable detection. We believe that the multi-resonance sensing performance has promising applications in biochemical molecular detection, and more generally, flexible modulation of spectra and light fields in optical devices.

Acknowledgements

C.Sun acknowledges support by Grant Number DLUXK-2024-YB-010 from the Interdisciplinary Project of Dalian University. This work was sponsored by National Laboratory of Solid State Microstructures, Nanjing University (M36007).

REFERENCES

1. **Kale, M.J., Christopher, P.** Plasmons at the Interface *Science* 349 (6248) 2015: pp. 587 – 588. https://doi.org/10.1126/science.aac852
2. **Pendry, J.B., Schurig, D., Smith, D.R.** Controlling Electromagnetic Fields *Science* 312 (5781) 2006: pp. 1780 – 1782. https://doi.org/10.1126/science.1125907
3. **Zhong, X., Rodrigo, S.G., Zhang, L., Samorì, P., Genet, C., Martín-Moreno, L., Hutchison, J.A. , Ebbesen, T.W.** Waveguide and Plasmonic Absorption-Induced Transparency *ACS Nano* 10 (4) 2016: pp. 4570 – 4578. https://doi.org/10.1021/acsnano.6b00709
4. **Zhang, S., Wong, C.L., Zeng, S., Bi, R., Tai, K., Dholakia, K., Olivo, M.** Metasurfaces for Biomedical Applications: Imaging and Sensing from a Nanophotonics Perspective *Nanophotonics* 10 (1) 2020: pp. 259 – 293. https://doi.org/10.1515/nanoph-2020-0373
5. **Yesilkoy, F., Arvelo, E.R., Jahani, Y., Liu, M., Tittl, A., Cevher, V., Kivshar, Y., Altug, H.** Ultrasensitive Hyperspectral Imaging and Biodetection Enabled by Dielectric Metasurfaces *Nature Photonics* 13 (6) 2019: pp. 390 – 396. https://doi.org/10.1038/s41566-019-0394-6
6. **Wang, B., Yu, P., Wang, W., Zhang, X., Kuo, H., Xu, H., Wang, Z.M.** High-Q Plasmonic Resonances: Fundamentals and Applications *Advanced Optical Materials* 9 2021: pp. 2001520. https://doi.org/10.1002/adom.202001520
7. **Chen, J., Gan, F., Wang, Y., Li, G.** Plasmonic Sensing and Modulation Based on Fano Resonances *Advanced Optical Materials* 6 2018: pp. 1701152. https://doi.org/10.1002/adom.201701152
8. **Yang, K., Yao, X., Liu, B., Ren, B.** Metallic Plasmonic Array Structures: Principles, Fabrications, Properties, and Applications *Advanced Materials* 33 (50) 2021: pp. e2007988. https://doi.org/10.1002/adma.202007988
9. **Cetin, A.E., Altug, H.** Fano Resonant Ring/Disk Plasmonic Nanocavities on Conducting Substrates for Advanced Biosensing *ACS Nano* 6 (11) 2012: pp. 9989 – 9995. https://doi.org/10.1021/nn303643w
10. **Park, J.H., Ndao, A., Cai, W., Hsu, L., Kodigala, A., Lepetit, T., Lo, Y.H., Kanté, B.** Symmetry-Breaking-Induced Plasmonic Exceptional Points and Nanoscale Sensing *Nature Physics* 16 2020: pp. 462. https://doi.org/10.1038/s41567-020-0796-x
11. **Braïk, M., Geronimi-Jourdain, T., Lau-Truong, S., Belkhir, A., Gam-Derouich, S., Chevillot-Biraud, A., Mangeney, C., Félidj, N.** Hybridization of Surface Lattice Modes: Towards Plasmonic Metasurfaces with High Flexible Tunability *Nanophotonics* 12 2023: pp.2179. https://doi.org/10.1515/nanoph-2023-0121
12. **Feng, T., Xiang, J., Liu, C., Geng, Z.** Gold Nano-Double-Ring Array Sensor Based on Fano Resonance *Optics Communications* 530 2023: pp. 129172. https://doi.org/10.1016/j.optcom.2022.129172
13. **Du, X., Xiong, L., Zhao, X., Chen, S., Shi, J., Li, G.** Dual-Band Bound States in the Continuum Based on Hybridization of Surface Lattice Resonances *Nanophotonics* 11 (21) 2022: pp. 4843 – 4853. https://doi.org/10.1515/nanoph-2022-0427
14. **Cuartero-González, A., Sanders, S., Zundel, L., Fernández-Domínguez, A.I., Manjavacas, A.** Super- and Subradiant Lattice Resonances in Bipartite Nanoparticle Arrays *ACS Nano* 14 (9) 2020: pp. 11876 – 11887. https://doi.org/10.1021/acsnano.0c04795
15. **He, Z., Li, Z., Li, C., Xue, W., Cui, W.** Ultra-High Sensitivity Sensing Based on Ultraviolet Plasmonic Enhancements in Semiconductor Triangular Prism Meta-Antenna Systems *Optics Express* 28 (12) 2020: pp. 17595 – 17610. https://doi.org/10.1364/OE.395640
16. **Chen, H., Lee, S., Montenegro, A., Kang, D., Gai, B., Lim, H., Dutta, C., He, W., Lee, M.L., Benderskii, A., Yoon, J.** Plasmonically Enhanced Spectral Upconversion for Improved Performance of GaAs Solar Cells under Nonconcentrated Solar Illumination *ACS Photonics* 5 (11) 2018: pp. 4289 – 4295. https://doi.org/10.1021/acsphotonics.8b01245
17. **Chu, S., Liang, Y., Yuan, H., Gao, H., Yu, L., Wang, Q., Peng, W.** Plasmonic Hybridization Generation in Self-

Aligned Disk/Hole Nanocavities for Multi-Resonance Sensing *Optics Express* 28 (24) 2020: pp. 36455 – 36465. https://doi.org/10.1364/OE.411773

18. **Palik, E.D.** Handbook of Optical Constants of Solids *Academic Press* 1998, 3.
19. FDTD Solutions, www.lumerical.com
20. **Sarkar, S., Ghosh, A., Adnan, M., Aftenieva, O., Gupta, V., Fery, A., Joseph, J., König, T.** Enhanced Figure of Merit via Hybridized Guided-Mode Resonances in 2D-Metallic Photonic Crystal Slabs *Advanced Optical Materials* 10 2022: pp. 2200954. https://doi.org/10.1002/adom.202200954
21. **Gantzounis, G., Stefanou, N., Papanikolaou, N.** Optical Properties of Periodic Structures of Metallic Nanodisks *Physical Review B* 77 2008: pp. 035101. https://doi.org/10.1103/PhysRevB.77.035101
22. **Liang, Y., Chu, S., Wei, X., Wei, H., Sun, C., Han, Y., Peng, W.** Substrate-Induced Hybridization of Plasmon Modes in the Composite Nanostructure of Nanodisk Array/Thin Film for Spectrum Modulation *Nanophotonics* 13 (21) 2024: pp. 3953 – 3961. https://doi.org/10.1515/nanoph-2024-0159